

Low background measurement in CANDLES-III for studying the neutrino-less double beta decay of ^{48}Ca

S. Ajimura,¹ W. M. Chan,¹ K. Ichimura,^{1,*} T. Ishikawa,¹ K. Kanagawa,¹ B. T. Khai,¹
 T. Kishimoto,¹ H. Kino,¹ T. Maeda,^{1,†} K. Matsuoka,¹ N. Nakatani,¹ M. Nomachi,¹
 M. Saka,¹ K. Seki,¹ Y. Takemoto,^{1,‡} Y. Takihira,¹ D. Tanaka,¹ M. Tanaka,¹ K. Tetsuno,¹
 V. T. T. Trang,¹ M. Tsuzuki,¹ S. Umehara,¹ K. Akutagawa,² T. Batpurev,² M. Doihara,²
 S. Katagiri,² E. Kinoshita,² Y. Hirano,^{2,§} T. Iga,² M. Ishikawa,² G. Ito,² H. Kakubata,²
 K. K. Lee,² X. Li,² K. Mizukoshi,^{2,¶} M. Moser,² T. Ohata,² M. Shokati,² M. S. Soberi,²
 T. Uehara,² W. Wang,² K. Yamamoto,² K. Yasuda,² S. Yoshida,² N. Yotsunaga,²
 T. Harada,³ H. Hiraoka,³ T. Hiyama,³ A. Hirota,³ Y. Ikeyama,³ A. Kawamura,³
 Y. Kawashima,³ S. Maeda,³ K. Matsuoka,³ K. Nakajima,³ I. Ogawa,³ K. Ozawa,³
 K. Shamoto,³ K. Shimizu,³ Y. Shinki,³ Y. Tamagawa,³ M. Tozawa,³ M. Yoshizawa,³
 K. Fushimi,⁴ R. Hazama,⁵ P. Noithong,⁵ A. Rittirong,⁵ K. Suzuki,⁶ and T. Iida⁷

(CANDLES Collaboration)

¹*Research Center for Nuclear Physics (RCNP),
Osaka University, Ibaraki, Osaka 567-0047, Japan*

²*Graduate School of Science, Osaka University, Toyonaka, Osaka 560-0043, Japan*

³*Graduate School of Engineering, University of Fukui, Fukui, 910-8507, Japan*

⁴*Department of Science and Technology, Tokushima
University, Tokushima, Tokushima 770-8506, Japan*

⁵*Department of Environmental Science and Technology,
Osaka Sangyo University, Daito, Osaka 574-8530, Japan*

⁶*The Wakasa-wan Energy Research Center, Tsuruga, Fukui 914-0192, Japan*

⁷*Faculty of Pure and Applied Sciences, University
of Tsukuba, Tsukuba, Ibaraki 305-8571, Japan*

Abstract

We developed a CANDLES-III system using 96 CaF_2 scintillation crystals with a total mass of 305 kg to study the neutrino-less double beta ($0\nu\beta\beta$) decay of ^{48}Ca . The system was equipped with a 4π active shield using a liquid scintillator to reject external backgrounds. The internal backgrounds caused by the radioactive impurities within the CaF_2 crystals can be effectively reduced by observing the signal pulse shape. We analyzed the data observed in the Kamioka underground for the live-time of 130.4 days to evaluate the feasibility of the low background measurement with the CANDLES-III detector. Moreover, we estimated the number of background events from the simulation based on the radioactive impurities in the CaF_2 crystals and the rate of high energy γ -rays caused by the (n, γ) reaction induced by environmental neutrons. The expected background rate was in a good agreement with the measured rate. In conclusion, the background candidates were properly estimated by comparing the measured energy spectrum with the background simulations. Consequently, no events were observed in the $Q_{\beta\beta}$ -value region when 21 high purity CaF_2 crystals were selected. This gave a lower limit on the half-life of $T_{1/2}^{0\nu\beta\beta} > 5.6 \times 10^{22}$ yr (90% confidence level) for the $0\nu\beta\beta$ decay of ^{48}Ca . With this measurement, we achieved the first $0\nu\beta\beta$ decay search in a low background condition with a detector using a Ca isotope, which was not enriched but natural, in a scale of hundreds of kg. The ^{48}Ca isotope has a high potential for the $0\nu\beta\beta$ decay search, and expected to be useful for the development of the next detector for a highly sensitive measurement.

* Present address: Research Center for Neutrino Science, Tohoku University

† Present address: Sector of Fukushima Research and Development, Japan Atomic Energy Agency

‡ Present address: Institute for Cosmic-ray Research, the University of Tokyo

§ Present address: Graduate School of Medicine, Nagoya University

¶ Present address: Department of Physics, Kobe University

I. INTRODUCTION

The remaining questions on the neutrino property are the absolute mass and its origin. These property can be potentially investigated by observing the neutrino-less double beta decay ($0\nu\beta\beta$ decay) [1]. A double beta ($\beta\beta$) decay has two modes. One is the two-neutrino $\beta\beta$ decay ($2\nu\beta\beta$ decay) accompanied with two electrons and two anti-neutrinos [2]. This decay mode is allowed within the standard model of particle physics and has been observed in several isotopes [3][4]. The other is the $0\nu\beta\beta$ decay, which can only occur if the neutrino is a Majorana particle [5]. This process is forbidden in the standard model because it violates the lepton number conservation law. The half-life of this decay is inversely proportional to the square of the effective Majorana neutrino mass; hence, the observation of the $0\nu\beta\beta$ decay establishes the Majorana nature of the neutrinos and gives the absolute scale of the effective neutrino mass [6] [7] [8].

The $0\nu\beta\beta$ decay has been searched using several isotopes [9], but has not yet been observed. Recent experiments have reported lower limits on the half-lives of $0\nu\beta\beta$ decays. The KamLAND-Zen and EXO-200 experiments have searched for the $0\nu\beta\beta$ decay of ^{136}Xe . They published results of the lower limit on the half-life of $T_{1/2}^{0\nu} \geq 1.07 \times 10^{26}$ yr for the KamLAND-Zen Collaboration [10], and 3.5×10^{25} yr for the EXO-200 Collaboration [11]. The GERDA and MAJORANA experiments have searched for the $0\nu\beta\beta$ decay of ^{76}Ge and set limits on the half-lives of $T_{1/2}^{0\nu} \geq 0.9 \times 10^{26}$ yr [12] and 1.9×10^{25} yr [13], respectively. The CUORE experiment has searched for the $0\nu\beta\beta$ decay of ^{130}Te and published the result on the half-life of $T_{1/2}^{0\nu} \geq 3.2 \times 10^{25}$ yr [14].

The $T_{1/2}^{0\nu}$ sensitivity scales linearly with the source mass (M) and the measurement time (t) in a background-free case, as opposed to \sqrt{Mt} in the case of background dominance. Thus, a background-free experiment is the key to scaling up the source volume and the measurement time. In this respect, the search for the $0\nu\beta\beta$ decay using the ^{48}Ca isotope is particularly promising because it has the highest Q-value ($Q_{\beta\beta}=4267.98 \pm 0.32$ keV [15]) among any $\beta\beta$ decaying isotopes. This $Q_{\beta\beta}$ -value is above the bulk of natural radioactive backgrounds and ensures a favorable phase space that enhances the $0\nu\beta\beta$ decay rate. Searches for the $0\nu\beta\beta$ decay of ^{48}Ca were firstly demonstrated approximately 60 years ago [16]. Since then, various measurements have been performed [17–23], no signals for the $0\nu\beta\beta$ decay were found in either measurements, with the best limit on ^{48}Ca currently set by the ELEGANT

VI experiment using 6.6 kg of $\text{CaF}_2(\text{Eu})$ scintillators (7.6 g of ^{48}Ca) at $T_{1/2}^{0\nu} \geq 5.8 \times 10^{22}$ yr [22]. The measurement was not limited by the backgrounds. The characteristic of the ELEGANT VI detector was the usage of a 4π active shield by its scintillator complex, and the success of which was the key to achieving a background-free measurement.

Our strategy for achieving better sensitivity is to increase a number of target nuclei and keep the background at a lower level, for which the initial concept of the CANDLES system is proposed. The Eu-doped CaF_2 used in ELEGANT VI has a large light output and gives a good energy resolution. However it has a short attenuation length because of the self-absorption of its scintillation light and is not suitable for the next step. A scale up with a good energy resolution without degrading the light collection can be achieved by utilizing the combination of undoped CaF_2 with a long attenuation length (more than 10 m) and the layer of the adjacent wavelength shifter (WLS). We realize a 4π active shield by surrounding the CaF_2 crystals in all directions with a luminous liquid scintillator (LS) to accomplish a background-free measurement. The highest $Q_{\beta\beta}$ -value combined with the 4π active shield achieved a substantial reduction of the backgrounds, which will be described in this paper.

The natural abundance of ^{48}Ca is denoted by the least amount of approximately 0.2% among the $\beta\beta$ decaying nuclei. On the contrary, this shows a big advantage of approximately 500 enhancement in case enrichment could be achieved, because CANDLES-III already reached a large volume of 300 kg. Several approaches for the ^{48}Ca enrichment are under development, including electromagnetic/optical separators [24], laser isotope separation [25], chemical separation [26] [27], and electrophoresis [28].

This article presents a method of achieving a low background condition. We will also show herein our first result of CANDLES-III in the Kamioka underground, which is comparable to the best result among the $0\nu\beta\beta$ measurements with ^{48}Ca . CANDLES has the potential to be the most competitive experiment, provided that an effective method for enriching ^{48}Ca and a detector with high energy resolution are available.

II. CANDLES-III DETECTOR

CANDLES (CALcium fluoride for the study of Neutrinos and Dark matters by Low Energy Spectrometer) is an experiment performed to search for the $0\nu\beta\beta$ decay of ^{48}Ca with undoped CaF_2 (CaF_2) scintillation crystals. The conceptual design of the CANDLES detector is

described in Ref. [29]. The current setup of the detector system, which is called CANDLES-III, is installed at lab-D in the Kamioka Underground Laboratory (2700 m.w.e.) in the Institute of Cosmic Ray Research of the University of Tokyo. Fig. 1 shows CANDLES-III system comprising 96 CaF_2 modules, a LS, a water buffer, 62 photomultiplier tubes (PMTs), and external shields.

The CaF_2 module consisted of a 10 cm cube (3.18 kg) undoped CaF_2 crystal, a 5 mm-thick layer of the WLS phase, and a 3 mm-thick acrylic container. In the WLS phase, the emission light of CaF_2 with a peak in the ultraviolet (UV) region was immediately converted to visible light, where the quantum efficiency of the PMTs was sufficient (maximum; ~ 400 nm), and the materials in the optical path had good transparencies [29]. The structure of the WLS phase surrounding the CaF_2 crystals was essential because the LS was not transparent to UV light. The WLS phase was composed of mineral oil in which WLS (Bis-MSB; 0.1 g/ ℓ) was dissolved. A total of 96 CaF_2 modules were arranged in six horizontal layers in the vertical direction, with the 16 CaF_2 modules on each layer in an acrylic tank (LS vessel) of a cylindrical shape of 1.4 m in diameter and 1.4 m in height. The layer number (N_l) and the module number (N_m) are defined in the Fig. 1 caption. The CaF_2 modules were suspended by wires from the ceiling of the LS vessel. Relatively radio-pure crystals were assembled in the central part of the detector based on the results of the commissioning runs [30–34]. The total mass of 96 CaF_2 crystals was 305 kg, in which included 350 g of ^{48}Ca .

The LS vessel was filled with the LS consisted of 80% mineral oil, 20% pseudo-cumene, and WLSs (PPO; 1.0 g/ ℓ and Bis-MSB; 0.1 g/ ℓ). The LS was used as an active shield, as will be described later. Prior to the commissioning run, we performed the LS purification process consisting of liquid–liquid extraction and nitrogen purge.

The scintillation lights from the CaF_2 modules and the LS were viewed by 62 PMTs (20-inch \times 14, 13-inch \times 36, and 10-inch \times 12). Fig.1 illustrates the configuration of three types of PMTs. Twenty-inch PMTs were installed on the top and bottom, and 13-inch and 10-inch PMTs were installed on the side in 4 rows and 12 columns. The 10-inch PMTs were used on the top row and the 13-inch PMTs were used on the other rows. A light collection system was installed between the PMTs and the LS vessel to improve the scintillation light collection [30]. The LS vessel and the PMTs were installed in a stainless-steel water tank of 3 m in diameter and 4 m in height. We employed cancellation coils outside the external shield to reduce the Earth’s magnetic field, which affects the charge collection efficiency

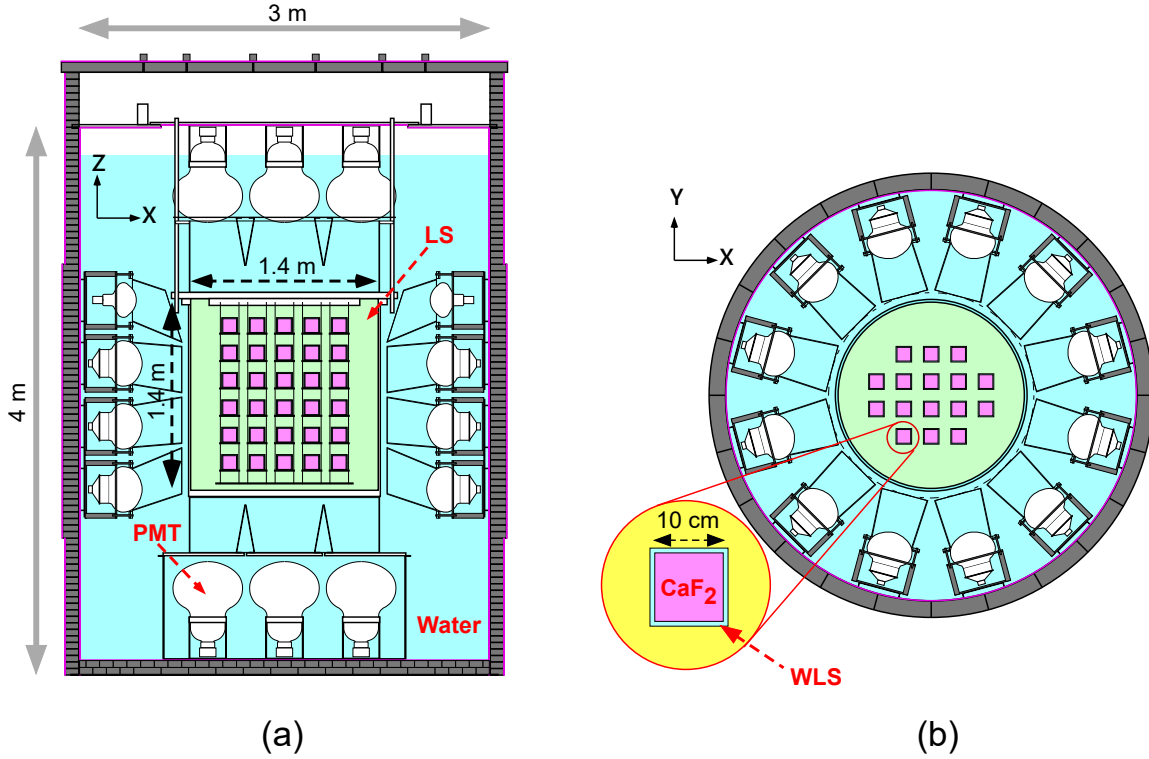


FIG. 1. Detector setup of CANDLES-III (a: side view and b: top view). A zoomed figure in (b) shows the details of a CaF_2 module. The layer number ($N_l = 1 - 6$) is from top to bottom. The module number ($N_m = 1 - 96$) first increases in the X-axis, and then in the negative Y and Z-axes. For the top layer ($N_l = 1$), $N_m = 1 - 16$. For the bottom layer ($N_l = 6$), $N_m = 81 - 96$. Here, the N_m of the zoomed CaF_2 module is 14.

of large-diameter PMTs. The coils were covered with a flame-retardant material. We also adjusted the coil current to reduce the Earth's magnetic field of ~ 400 mG to below 60 mG in average at every PMT position based on a magnetic field simulation. A high-voltage power supply for the PMTs and the current supplies for the cancellation coils with the interlock were installed in the DAQ hut.

The whole detector was covered with external passive shields to reduce the high energy γ -rays produced by the environmental neutron capture reactions ((n,γ) reaction) in the detector materials and rocks [35].

We employed the Pb shield (gray bricks, Fig. 1) outside of the water tank for the γ -

ray produced by (n,γ) reaction on rocks. The typical Pb thickness was 10 cm to reduce γ -rays with several MeVs by 1/100. Considering a more effective reduction of the external background, Pb thickness was 12 cm in the center of the detector side, where the passive water shield was relatively thin.

The stainless-steel water tank was another source of high energy γ -ray. Accordingly, Si rubber sheets containing 40 wt.% of B_4C (B sheet, purple sheets shown in Fig. 1) were attached both inside and outside of the tank to prevent (n,γ) reaction inside the Pb shield. The B sheet thickness of 4 mm was enough to reduce the thermal neutrons by approximately 1/1000.

A detector cooling system was installed to increase the scintillation light output emitted by CaF_2 . The light output from the undoped CaF_2 increased by 2% with the temperature decrease of 1 °C around room temperature [36]. The lab-D temperature was cooled down to a temperature slightly higher than the freezing point of water used as the passive shield (2 °C for setting temperature). Consequently, the center of the detector was cooled down to 4.5 °C and stabilized within ± 0.05 °C. The light output of CaF_2 was increased by approximately 30% compared in the case of operating at room temperature. The stabilized temperature led to no detectable change of gain caused by the temperature [33].

For a long-term stable measurement, a monitoring system for the laboratory environment (e.g., temperature, humidity, atmospheric pressure in the lab-D, water temperatures inside the water tank, temperature and humidity in the DAQ hut, etc.) was installed, and the data were continuously recorded. The liquid levels of water and LS were constantly monitored. We also installed leak detectors for water and LS and connected their alarm signals to the interlock of the power supplies for a safe operation of the detector containing a flammable substance (i.e., LS).

The DAQ system consisted of hardware including Flash ADCs (FADCs), and a trigger logic on the μ TCA system, and a network DAQ software. The signal waveform for each PMT was recorded for approximately 9 μ sec by an 8-bit 500 MHz FADC [37]. The waveform was recorded in a 2 nsec time-bin for the first 768 nsec and in a 64 nsec time-bin, which was the sum of 32 samples of 2 nsec time-bin data, for 8.2 μ sec with a time stamp. It was read through a SpaceWire datalink [38] on the μ TCA backplane. The pulse shape digitized from the analog waveform was used in an offline analysis of the background reduction through pulse shape discrimination.

We developed a dual-gate trigger system to efficiently collect the long decay-time signals by rejecting the LS signals with short decay-times [39]. The signals were integrated into two different time windows (“dual gate”) in the FPGA, and triggered only when both integrated values exceed each threshold.

A random trigger event using a pulser was acquired at 3 Hz. A single photoelectron event, which accidentally entered in a random trigger event, was collected. The charge-photoelectron conversion coefficient was calculated for each PMT every 24 hours by taking the average value of the FADC counts of single photoelectron events.

The energy threshold was set to tag the α decay of $^{212}\text{Bi} \rightarrow ^{208}\text{Tl}$. This α -ray of 6.05 MeV caused a scintillation that was of the same amount as the β -ray of 1.63 MeV due to the CaF_2 scintillation quenching. The energy thresholds for each CaF_2 module were distributed between 0.8 and 1.2 MeV (Fig. 15 in Ref. [39]) to detect the α -ray of ^{212}Bi and identify the subsequent ^{208}Tl decay.

The software we developed herein was based on a system using the DAQ-Middleware framework and an online monitoring system [40][41]. The FADC data were collected by the fast reader components installed in a personal computer (PC) via the SpaceWire to the Gigabit Ethernet interface. The slow data (H.V. values, temperatures, etc.) were collected by slow reader components installed in another PC. The data were partly analyzed for the online monitoring system and fully recorded to a hard disk for the offline analysis.

III. PARAMETERS AND DETECTOR PERFORMANCE FOR DATA ANALYSIS

A. Pulse shape analysis

In the analysis of the CANDLES-III experiment, pulse shape discrimination (PSD) parameters were used to discriminate the following β -rays and γ -rays events that deposited energy only in the CaF_2 crystals (β -events); events involving LS emission (β +LS-events) to realize a 4π active shield; and α -ray events in CaF_2 (α -events) for the background rejection analysis.

The LS acted as an active shield for the immersed CaF_2 modules to reduce the background events accompanied by the γ -rays. The active shield was achieved by observing the pulse shapes. The decay-time of CaF_2 scintillation was 1 μsec , whereas that of the LS was typically

a few tens of nanoseconds. The events from the $0\nu\beta\beta$ decay led to an energy deposit only in CaF_2 , while the background events accompanied by the γ -rays can yield energy deposits in the LS as well as in CaF_2 (β +LS-events). The pulse shape of the β +LS-events had a large prompt component, whereas that of the $0\nu\beta\beta$ candidate signals did not, as shown in Fig. 2. Thus, by observing the pulse shapes, the background signals of the β +LS-events can be discriminated as yielding a certain amount of energy deposits in the LS.

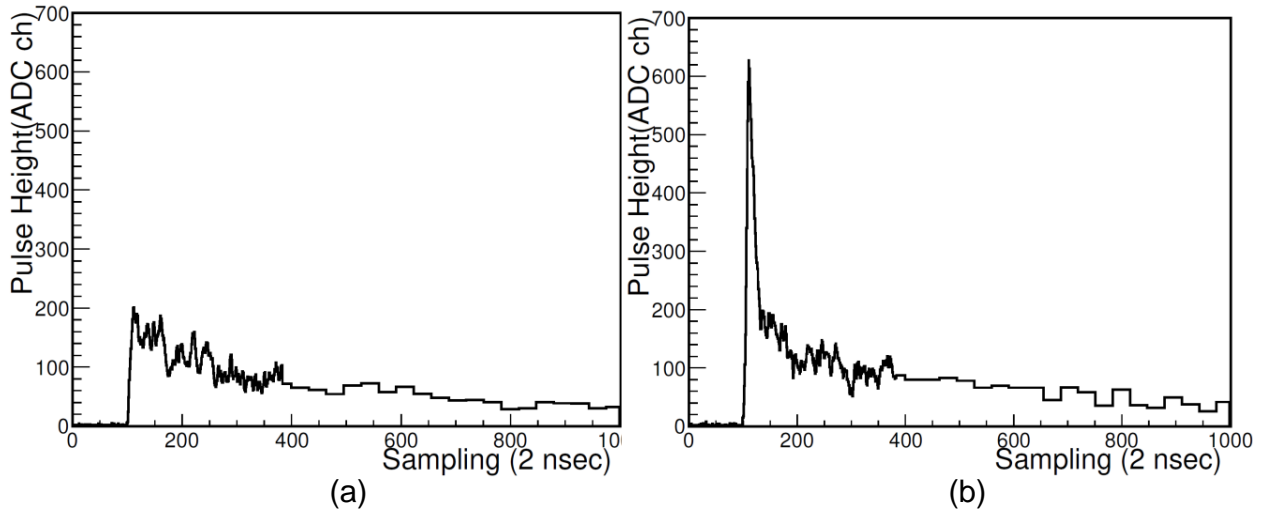


FIG. 2. Scintillating pulse shape observed with the CANDLES-III detector. The recorded waveforms with 62 PMTs are summed up. The data were recorded in a 2 nsec time-bin for the former 768 nsec region and a 64 nsec time-bin for the latter region. The energy deposits of both events are ~ 2.6 MeV. (a) Observed pulse shape with CaF_2 without any energy deposit in the LS. (b) Pulse shape of a background event in coincidence with the LS.

The other major backgrounds in CANDLES-III were the ^{208}Tl decay and the $^{212}\text{Bi} \rightarrow ^{212}\text{Po} \rightarrow ^{208}\text{Pb}$ sequential decay within the CaF_2 crystal. Alpha-rays were involved in these background reduction because ^{212}Po emitted an α -ray, and the ^{208}Tl decays were preceded through the α -ray by the ^{212}Bi decay, as described detail in Section IV A. Thus, identifying α -events is important for the background reduction. CaF_2 can discriminate between α - and β -events based on the characteristics of the prompt part of the signal pulse shape [30].

1. Reference pulse shape for the PSD

Three types of average pulse shape of the β -events in the CaF_2 crystal, LS-events, and α -events were created as the reference. The PSD analysis was performed by comparing the pulse shapes of each event with the references.

The reference pulse shape of the β -events was made using 2.615 MeV γ -rays from the ^{208}Tl decays that deposited energy only in the CaF_2 crystal. The events yielding 2.615 MeV energy deposit only in CaF_2 were caused by the γ -rays from the ^{208}Tl decays outside the LS vessel (PMT, etc.). In other words, the γ -rays always passed through the LS and frequently deposited energy in the LS. The light yield of the LS was smaller than that of the CaF_2 module; thus, the multiple scattering events in both CaF_2 and LS distributed a lower energy region when compared to the peak of the γ -ray (2.615 MeV). The events in the energy window between 2.64 and 2.77 MeV were used to select the β -events with a negligible amount of energy deposit in the LS. We evaluated the bias in making the reference pulse shape of the β -events, where only the events in the higher energy region of the γ -ray peak were selected. The pulse shape from CaF_2 alone was taken by the detector setup without the LS installation. The reference pulse shape was made by the γ -rays from the ^{208}Tl decays selected by the same cut condition in the full CANDLES-III setup. The obtained average pulse shape without the LS was consistent with the reference pulse shape made by the method mentioned above. The light yield, light collection, and detector temperature of the setup without the LS were different from those in the full setup. Therefore the reference pulse shape of the β -events in the full setup was used for the PSD analysis.

The events with an energy deposit above 300 keV only in the LS were used to make the reference pulse shape of the LS-events. At the same time, only the events near the detector center were selected because the pulse shape recorded by the PMT near the LS-event overflowed. The LS-events were taken by different trigger conditions by applying only the pulse height threshold because the dual-gate trigger effectively collected the events with energy deposit in the CaF_2 crystal.

The α -events by the ^{215}Po decay (^{235}U series) contained in the CaF_2 crystal were used to make the reference pulse shape because the ^{215}Po decay can be correctly selected by the delayed coincidence analysis of $^{219}\text{Rn} \rightarrow ^{215}\text{Po}$ ($T_{1/2} = 1.781$ msec) $\rightarrow ^{211}\text{Pb}$. In addition, the ^{215}Po decay accompanied almost no γ -rays. The pure α -event reference pulse shape can

be obtained.

2. PSD parameters

Two types of PSD analysis were performed using each signal pulse shape within 500 nsec from the starting time of the pulse shape, where the reference pulse shapes were particularly different among the α -, β -, and β +LS-events. The first analysis aimed to remove the β +LS-events. Meanwhile, the second analysis used a shape indicator (SI) [42] to discriminate between the α - and β -events in CaF_2 .

We removed the β +LS-event by performing a chi-square test of each event pulse shape. The 500 nsec to 4000 nsec interval from the starting time of pulse shape was fitted using the reference pulse shape of a β -event (i.e., normalizing the reference pulse shape to the pulse height of each event). The chi-square of each event pulse shape to the reference pulse shape was calculated in the 2 nsec time-bin region up to 500 nsec. In obtaining the chi-square, an error was given by the number of the photoelectrons converted from the pulse height. The chi-square calculated using only the reference pulse shape of the β -events was presented as PSD_β , while that calculated using both the reference pulse shapes of the β - and LS-events was denoted by $\text{PSD}_{\beta+\text{LS}}$. At this time, the pulse height of the reference pulse shape of the LS-events was also fitted such that the $\text{PSD}_{\beta+\text{LS}}$ was minimized to evaluate the energy deposit in the LS.

Fig. 3(a) shows the PSD_β distribution obtained for the β -events with an energy deposit of 2.615 MeV and the β +LS-events. The pulse shape of the β +LS-events was artificially created by randomly combining a β -event with 2.6 MeV and an LS-event with 140 keV. The β -events peaked at 1 in the PSD_β distribution, and the β +LS-events were distributed at large values, and vice versa, taking $\text{PSD}_{\beta+\text{LS}}$. Fig. 3(b) shows the discrimination ability between the β - and β +LS-events for each energy deposit in the LS at around 2.6 MeV, where the γ -rays from the ^{208}Tl decay were observed. When the energy deposit of the LS was 140 keV (approximately 5% of the total observed energy), the β +LS-events can be discriminated with a separation level of more than $3\bar{\sigma}$, where $\bar{\sigma}$ is defined as $\sqrt{\sigma_\beta^2 + \sigma_{\beta+\text{LS}}^2}$.

We adopted the SI for the PSD analysis to discriminate between α - and β -events in CaF_2 . The SI obtained by weighting to emphasize the difference had a better discrimination ability. The α -events can be discriminated from the β -events at the 4σ level in the 2.6 MeV region,

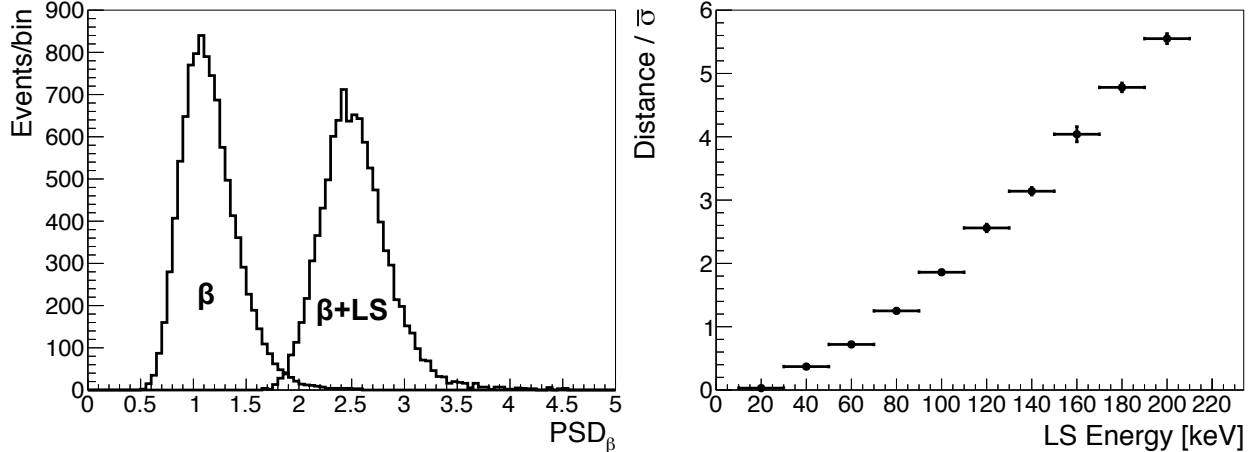


FIG. 3. Separation of the β - and β +LS-events by the PSD analysis: (a) illustration of the PSD_β distribution of the β - and β +LS-events and (b) LS energy dependence on the discrimination ability obtained by the same analysis as in (a) at different LS energies.

which corresponds with the energy of 7.7 MeV for the α -ray (Fig. 3 of Ref. [30]).

B. Position reconstruction

The position reconstruction and the crystal determination of an event, in which the event deposits energy (hit-crystal), are important for the energy reconstruction and background rejection. The position was reconstructed event by event with signals from 62 PMTs. The pedestal was calculated in the first 180 nsec before the starting time of the pulse shape (Fig. 2). Subtracting the pedestal, integrating over the range of 4 μ sec from the starting time to obtain the charge, and converting it to the number of photoelectrons detected by each PMT.

The position was determined by the following formula using the light yield centroid method:

$$\overrightarrow{\text{Position}} = \frac{\sum_{i=1}^{62} (N_{pe}(i) \times \overrightarrow{\text{PMT}}(i))}{\sum_{i=1}^{62} N_{pe}(i)}. \quad (1)$$

Here, $N_{pe}(i)$ is the number of photoelectrons observed in each PMT, and $\overrightarrow{\text{PMT}}(i)$ depicts the position coordinates of each PMT. Fig. 4 shows a two-dimensional plot of the reconstructed position for the β -events caused by the γ -rays from the ^{40}K decays mostly contained in the PMTs. Each cluster corresponded to a crystal. The hit-crystal was unambiguously

determined. Subsequently Gaussian fitting was performed for each crystal on three axes. Its mean and sigma values were then evaluated. Consequently, the peak-to-peak distance between the crystals was found to be 7–8 sigma. The mean and sigma values obtained here were used in the analysis for the hit-crystal determination.

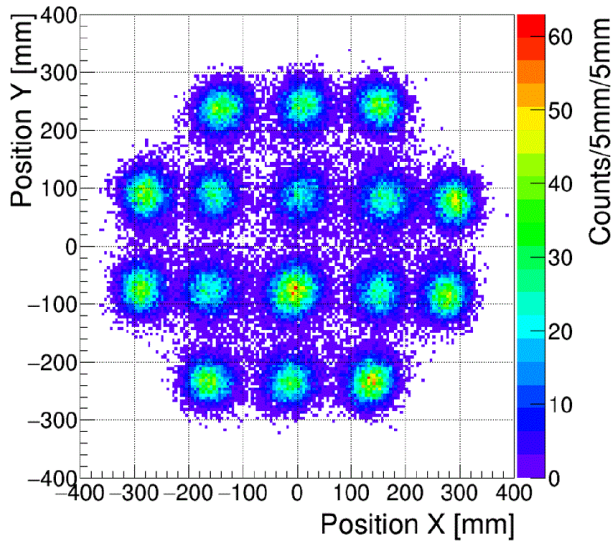


FIG. 4. Two-dimensional distribution of the reconstructed position (X versus Y direction). The actual distance to the adjacent crystal is 20 cm, but the reconstructed position is not corrected for that distance.

C. Energy reconstruction and energy calibration

The amount of light yield for each CaF_2 module was slightly different from each other, and the light collection efficiency differed depending on the position. The hit-crystal was determined by the reconstructed position, and then the energy for each event was determined based on the number of photoelectrons using the following formula:

$$\text{Energy} = \sum_{i=1}^{62} N_{pe}(i) \times C_{relative}(N_m) \times C_{fine}(N_l). \quad (2)$$

Here, $C_{relative}$ is a photoelectron-energy conversion coefficient determined for each CaF_2 module, and C_{fine} is a fine correction coefficient for the energy scale linearity in the high energy region determined for each layer. N_m and N_l represent the module and layer numbers, respectively.

We performed a relative energy calibration for each CaF_2 module with 1.836 MeV γ -ray of an ^{88}Y source to determine $C_{relative}(N_m)$. Coefficient C_{fine} was estimated for the whole data period with the background events of the ^{208}Tl γ -ray (2.615 MeV). The energy scale and the resolution near the $Q_{\beta\beta}$ -value were evaluated using 3 to 9 MeV γ -rays emitted by the neutron captures on the Si, Fe, and Ni nuclei using a ^{252}Cf neutron source.

A calibration run was performed with the ^{88}Y source inserted into the LS vessel and placed between the CaF_2 modules. The data were collected at 18 locations in the detector to sufficiently irradiate all the 96 modules with γ -rays. Fig. 5 plots the average number of photoelectrons for each crystal at 1.836 MeV γ -ray. Accordingly, $C_{relative}$ was calculated to correct this variation.

The energy scale was then corrected using the background peak caused by 2.615 MeV γ -rays from ^{208}Tl decays. Despite the relative correction between the CaF_2 modules, a few % of the energy scale dependence existed on the Z direction of the detector. The cause of the layer dependence was unknown, but it was considered herein to be the asymmetry in the Z direction of the detector (PMT sizes, etc.). After this fine correction, the energy scale uniformity of all the crystals was confirmed using 1.461 MeV γ -rays of ^{40}K in the physics run data.

Finally, the calibration was performed in the energy region above 3 MeV using the γ -rays emitted by the neutron capture reaction of ^{28}Si and ^{58}Ni . This calibration was performed once per whole data taking term. Polyethylene bricks mixed with Si or Ni powder were made and assembled inside the Pb shield on top of the water tank. A ^{252}Cf source was placed in the center of the bricks to generate neutron capture γ -rays. The calibration results showed that the systematic error of the energy scale at the Q -value was less than 0.3%. Furthermore, the energy resolution at the $Q_{\beta\beta}$ -value was $\sigma = 2.4\%$. The details of the system and the analysis results were discussed in Ref. [43].

After all the calibrations, the energy scale stability was confirmed every 24 hours using the ^{208}Tl peak. Its stability was found to be better than 0.3% for the live-time.

IV. BACKGROUND ANALYSIS

This chapter describes the detailed characteristics of the backgrounds relevant to CANDLES-III. Each background rate was calculated using a Monte Carlo simulation. We performed the

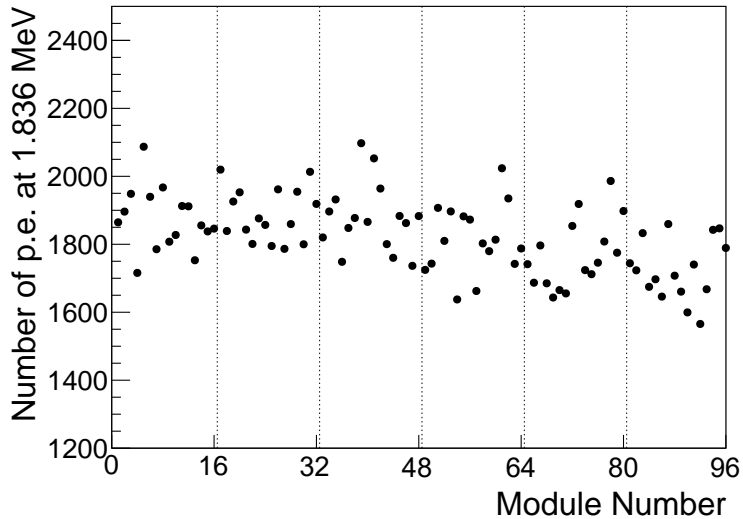


FIG. 5. Average number of photoelectrons for 1.836 MeV γ -ray of ^{88}Y as a function of the module number. The 16 modules between two vertical dotted lines correspond to one layer.

analysis using the experimental data for the live-time of 130.4 days to confirm the feasibility of CANDLES-III for low background measurement.

A. Background candidates

The backgrounds around the $Q_{\beta\beta}$ -value were identified by event information, such as energy, position (i.e., hit-crystal), timing, and signal pulse shape. The background origins were limited to the following three sources since the $Q_{\beta\beta}$ -value was sufficiently high.

1. (n,γ) reaction

The environmental neutron produced many γ -rays, whose energies exceeded the $Q_{\beta\beta}$ -value of ^{48}Ca . Many events above the $Q_{\beta\beta}$ -value were observed. Prominent peaks were particularly observed around 7 – 8 MeV in the initial run of CANDLES-III before the Pb shield construction. The background origin was identified to be the high energy γ -rays produced by the neutron capture in the surrounding materials. A rock containing Si and Fe isotopes was largely abundant. A high energy γ -ray was occasionally absorbed by a single CaF_2 crystal because of its large size (10 cm cube). The environmental neutrons were

induced by an (α, n) interaction in the surrounding rocks. The α -rays were produced by the decays of the progenies of the ^{238}U and ^{232}Th contents in the rocks. The neutron-induced background was reduced by installing the Pb shield outside of the water tank, as described in Section II.

The high energy γ -ray events were almost rejected by the PSD_β analysis. The remaining events caused by the high energy γ -rays were estimated by the experimental data obtained by irradiating an artificial neutron source. The details of the (n, γ) background estimation were described in Ref. [35]. The background rate by the neutron captured in the surrounding rocks was estimated as 0.9 ± 0.6 events for the live-time.

2. ^{208}Tl decay

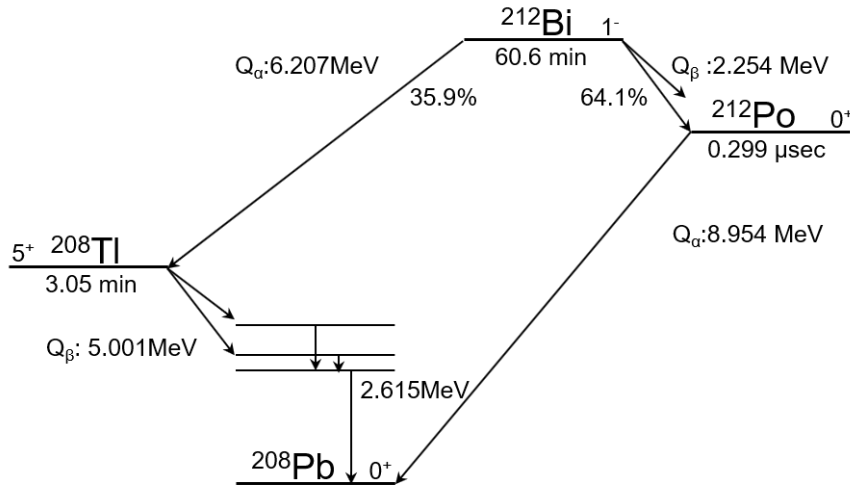


FIG. 6. Last part of the ^{232}Th series from ^{212}Bi to ^{208}Pb . ^{208}Tl always decays into the excited states of ^{208}Pb , then decays into the ground state with 2.615 MeV γ -ray emission.

The ^{208}Tl decay in the CaF_2 crystal was another background candidate for the $0\nu\beta\beta$ decay search, because the Q -value (5.001 MeV) was above the $Q_{\beta\beta}$ -value of ^{48}Ca . ^{208}Tl did not directly decay to the ground state, but to the excited states of ^{208}Pb , thereby always emitting 2.615 MeV γ -rays (Fig. 6). Most of the events induced by the ^{208}Tl decay were removed by the PSD_β analysis because the γ -ray of 2.615 MeV caused multiple scattering in both CaF_2 and the LS. However, it became a background when the β -ray and γ -ray (2.615 MeV) from ^{208}Tl decay were fully absorbed in the same CaF_2 crystal. Such event

can be effectively identified by tagging the preceding α decay of $^{212}\text{Bi} \rightarrow ^{208}\text{Tl}$. The α -ray of ^{212}Bi was followed by the β decay of ^{208}Tl ($T_{1/2} = 3.05$ min). The α -ray with 6.05 MeV energy was observed at 1.63 MeV in the energy scale determined by the energy calibration (Section III C) because of the CaF_2 scintillation quenching. When the β -ray and γ -ray (2.615 MeV) from ^{208}Tl decay were absorbed by different CaF_2 crystals, the event position was reconstructed in the LS area, and not in the CaF_2 crystal. These multi-crystal events were rejected by the position reconstruction analysis.

3. $^{212}\text{BiPo}$ event

The ^{212}Bi decays to ^{212}Po had a branching ratio of 64% (Fig. 6). The half-life of ^{212}Po ($T_{1/2} = 0.299$ μsec) was shorter than the decay-time of the CaF_2 scintillation (1 μsec); hence, the delayed ^{212}Po α decay piled up the prompt ^{212}Bi β decay. This sequential decay was observed as one event when the time-lag of the decays was relatively short and distributed in the energy region up to 5.1 MeV [30], since the ^{212}Po α -ray was observed at 2.88 MeV due to the quenching effect. The sequential decay of $^{212}\text{Bi} \rightarrow ^{212}\text{Po} \rightarrow ^{208}\text{Pb}$ ($^{212}\text{BiPo}$ event) made the background for the $0\nu\beta\beta$ decay search.

B. Background rejection and $0\nu\beta\beta$ decay analysis

The criteria for selecting the candidate events for the $0\nu\beta\beta$ decay are given as follows:

- (1) CaF_2 signal without energy deposit in the LS;
- (2) not a sequential signal caused by the $^{212}\text{BiPo}$ event;
- (3) not a candidate of the ^{208}Tl decay; and
- (4) reconstructed event at the CaF_2 crystal position.

As mentioned in section III A, criterion (1) was applied using the PSD analysis to remove β +LS events.

Criterion (2) was applied by analyzing the pulse shape [30]. The $^{212}\text{BiPo}$ event was easily recognized as a sequential event when the time-lag was longer than 20 nsec since the typical rise-time of the CaF_2 signal was 20 nsec. The events with time-lags shorter than 20 nsec were rejected using SI to discriminate between the β - and α -events. This was because a large portion of the pulse shape was caused by the ^{212}Po α -events. The total rejection efficiency

of the $^{212}\text{BiPo}$ events was more than 99%.

Criterion (3) was applied by a time correlation analysis between the ^{212}Bi α decay and ^{208}Tl β decay. The ^{212}Bi α -ray was identified by the SI and its energy (1.63 MeV). The timing and the hit-crystal of the α -events were recorded. The event observed in the identical crystal and within 18 minutes after the α -event was tagged as the $^{212}\text{Bi}\rightarrow^{208}\text{Tl}\rightarrow^{208}\text{Pb}$ event [34]. The rejection efficiency of the ^{208}Tl decays by this α -tagging analysis was 89%.

The event, in which the 2.615 MeV γ -ray was absorbed in the other CaF_2 crystal as a ^{208}Tl β -ray, can be rejected through criterion (4). This multi-crystal event might be reconstructed in the position of the LS area. To apply criterion (4), we selected the events within the $\pm 2\sigma$ region from the center of each CaF_2 crystal, as presented in Section III B.

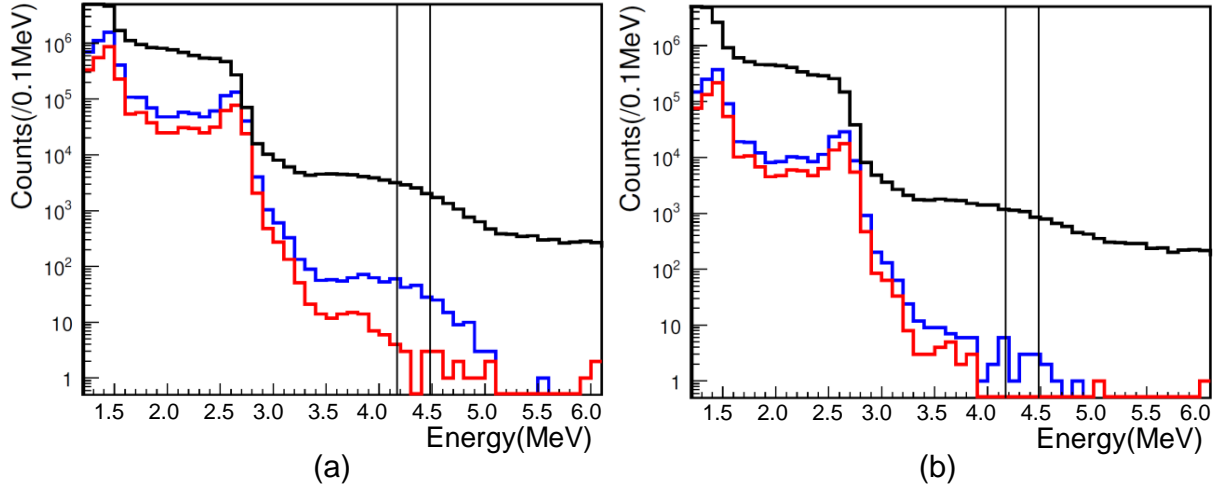


FIG. 7. Obtained energy spectra with each event selection using (a) 93 CaF_2 crystals and (b) 21 high purity CaF_2 crystals. The black lines correspond to the raw events without any selections. The blue lines correspond to those with selection criteria (1) and (2). The red lines correspond to those with criteria (1) – (4). The details of the event selection criteria (1) – (4) are described in the text. The region between two vertical lines represents the $0\nu\beta\beta$ window of 4.17 – 4.48 MeV. After the event selections, no events are observed in the $Q_{\beta\beta}$ -value region when 21 high purity crystals are selected.

Figs. 7(a) and (b) show the energy spectra obtained by applying the selection criteria with 93 and 21 CaF_2 crystals, respectively. We used the 93 CaF_2 crystals for the $0\nu\beta\beta$ decay analysis because three CaF_2 crystals out of the 96 had poor performance. The 21 CaF_2 crystals were selected as high purity crystals, whose radioactive impurities of ^{232}Th

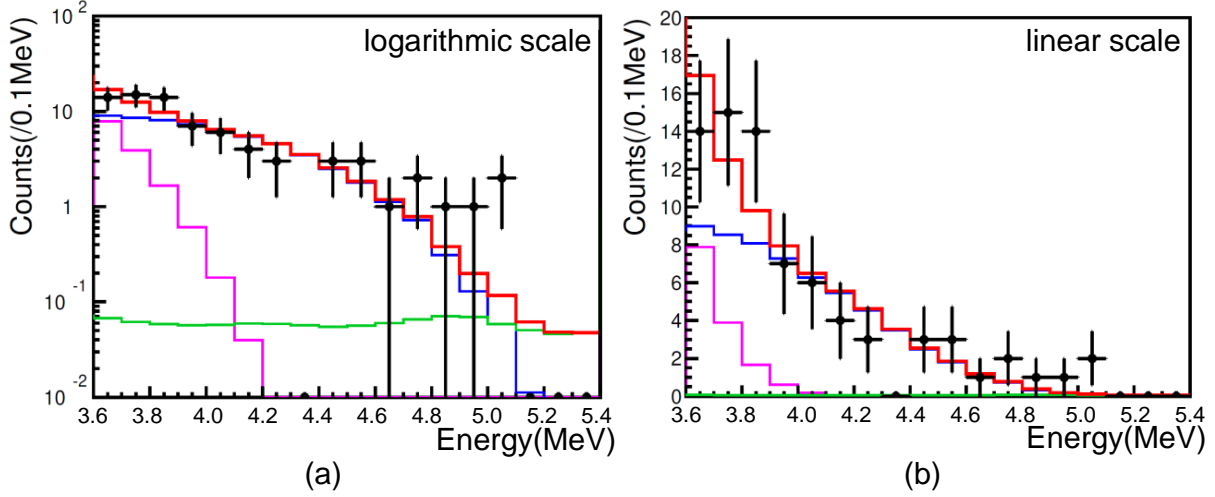


FIG. 8. Obtained energy spectra (plots) and simulated background spectra (lines) obtained by using 93 CaF_2 crystals. The blue, magenta, and green lines correspond to the simulated background spectra of ^{208}Tl and $^{212}\text{BiPo}$, $2\nu\beta\beta$ decay, and (n,γ) events, respectively. The red line represents the summed up spectrum of all three simulated spectra. The right spectra present the same as the linear scale. The experimental energy spectrum in the $Q_{\beta\beta}$ -value region is well reproduced by the simulated one.

series were less than $10 \mu\text{Bq/kg}$. The blue lines in the figures correspond to the events with criteria (1) and (2), which were required for rejecting the β +LS-events. The event rates of the blue lines were less than those of the black lines by more than two orders of magnitude above 3.5 MeV, indicating that the LS efficiently worked as a 4π active shield for the CaF_2 crystals to reduce the external backgrounds. The red spectra in Figs. 7 were obtained by applying event selection criteria (1) – (4). We observed no events in the $0\nu\beta\beta$ window of 4.17 – 4.48 MeV for the selected 21 CaF_2 crystals, whereas six events were observed for the 93 CaF_2 crystals.

The detection efficiencies of the $0\nu\beta\beta$ decay applying PSD analyses were estimated to be 70.9% and 71.8% for the 93 and 21 CaF_2 crystals, respectively. These efficiencies were reduced to 49.3% by selecting events in the $0\nu\beta\beta$ window for both CaF_2 crystal cases. The events within 18 minutes after the ^{212}Bi α -rays candidate detection were rejected by applying criterion (3). The live-time of the data was reduced to 72.7% and 76.1% for the 93 and 21 CaF_2 crystals, respectively.

Fig. 8 shows the simulated background and measured spectra with the 93 CaF₂ crystals. The red-colored spectrum represents the sum of the simulated background spectra, comprising ²¹²BiPo events, ²⁰⁸Tl decays, γ -rays by neutron capture reactions, and $2\nu\beta\beta$ decays with the half-life of $T_{1/2}^{2\nu\beta\beta} = 5.3 \times 10^{19}$ year [4]. We considered the following parameters for the background rate estimation: (1) concentration of the radioactive impurities of the ²³²Th series in each CaF₂ crystal determined by the time-correlation analysis of the decays ²²⁰Rn \rightarrow ²¹⁶Po ($T_{1/2} = 145$ msec) \rightarrow ²¹²Pb; (2) detection efficiency of the event selection criteria; and (3) detector energy resolution [43]. We obtained the estimated background rate of 27.1 counts/130.4 days/(93 CaF₂ crystals) within the 4–5 MeV region (Fig. 8). The estimated background rate was consistent with the measured rate of 24 events. This fact strongly supported our hypothesis that the considered three background candidates were the major candidates in the CANDLES-III detector.

We can set a lower limit and an experimental sensitivity on the half-life of the $0\nu\beta\beta$ decay by using the expected background rate of 1.0 counts in the $0\nu\beta\beta$ window of 4.17 – 4.48 MeV for the 21 CaF₂ crystals. The half-life limit with 90% C.L. obtained by selecting 21 CaF₂ crystals was 5.6×10^{22} year. This limit was comparable to the result obtained for more than 2 years using our previous detector, ELEGANT VI[22]. We also obtained an experimental sensitivity of 2.7×10^{22} year (90% C.L.) because the observed event rate was lower than expected. The obtained half-life limit derived an upper limit on the effective Majorana neutrino mass $\langle m_\nu \rangle \leq 2.9 - 16$ eV (90% C.L.) using the nuclear matrix elements given in Ref. [44] and the reference therein.

The present limits on the half-life and the effective Majorana mass were obtained using natural Ca instead of enriched ⁴⁸Ca crystals. The limit on $\langle m_\nu \rangle$ did not reach sufficient sensitivity compared with the experiments using other enriched $\beta\beta$ isotopes, such as ⁷⁶Ge and ¹³⁶Xe, because of the lack of ⁴⁸Ca isotope amount overcome by realizing ⁴⁸Ca enrichment. The results obtained herein demonstrated that ⁴⁸Ca is a promising isotope that is sufficiently competitive in other sensitive experiments.

V. CONCLUSION

This study evaluated the feasibility of low background measurements with the CANDLES-III detector using the live-time of 130.4 day data. We confirmed that the structure of the 4π

active shield and the passive shields can effectively reduce the external backgrounds. The backgrounds caused by the radioactive impurities of the ^{232}Th series contained in the CaF_2 crystals can be effectively removed by analyzing the signal pulse shape and tagging the time correlated α decay. After the background rejection analyses, no events in the $Q_{\beta\beta}$ -value region were found when we selected high purity 21 CaF_2 crystals. This gave a lower limit on the half-life of the $0\nu\beta\beta$ decay of ^{48}Ca as $T_{1/2}^{0\nu\beta\beta} > 5.6 \times 10^{22}$ yr (90% C.L.), which was almost comparable with the limit obtained by ELEGANT VI over two years of long-term data [22]. We also presented the experimental sensitivity of 2.7×10^{22} yr (90% C.L.) by the predicted background rate. The observed energy spectrum around the $Q_{\beta\beta}$ -value region was well reproduced by the simulated one, which estimated by the three background candidates considered. In other words, there were likely no additional high-impact backgrounds. The present result is useful for the development of the next detector and shows that ^{48}Ca is a promising target nucleus for the $0\nu\beta\beta$ decay search using CaF_2 crystals.

ACKNOWLEDGMENTS

This work was supported by JSPS/MEXT KAKENHI Grant Number 19H05804, 19H05809, 26104003, 16H00870, 24224007, and 26105513. This work was supported by the research project of Research Center for Nuclear Physics (RCNP), Osaka University. This work was also supported by the joint research program of the Institute of Cosmic Ray Research (ICRR), the University of Tokyo. The work of KT was supported by JSPS Research Fellowship for Young Scientists. The Kamioka Mining and Smelting Company has provided service for activities in the mine.

-
- [1] W. H. Furry, Phys. Rev. **56**, 1184 (1939).
 - [2] M. Goepfert-Mayer, Phys. Rev. **48**, 512 (1935).
 - [3] A. S. Barabash, Phys. Rev. **C81**, 035501 (2010).
 - [4] A. S. Barabash, AIP Conference Proceedings **2165**, 020002 (2019).
 - [5] E. Majorana, Nuovo Cim. **14**, 171 (1937).
 - [6] J. Schechter and J. W. F. Valle, Phys. Rev. D **25**, 2951 (1982).
 - [7] H. Ejiri *et al.*, Phys. Rep. **797**, 1 (2019).

- [8] H. Ejiri, *Frontiers in Physics* **7:30**, 1 (2019).
- [9] M. Dolinski *et al.*, *Annu. Rev. Nucl. Part. Sci.* **69**, 219 (2019).
- [10] A. Gando *et al.* (KamLAND-Zen Collaboration), *Phys. Rev. Lett.* **117**, 082503 (2016), [Addendum: *Phys. Rev. Lett.* **117**, no.10, 109903 (2016)].
- [11] G. Anton *et al.* (EXO-200), *Phys. Rev. Lett.* **123**, 161802 (2019).
- [12] M. Agostini *et al.* (GERDA Collaboration), *Science* **365**, 1445 (2019).
- [13] C. E. Aalseth *et al.* (Majorana Collaboration), *Phys. Rev. Lett.* **120**, 132502 (2018).
- [14] D. Q. Adams *et al.* (CUORE Collaboration), *Phys. Rev. Lett.* **124**, 122501 (2020).
- [15] A. A. Kwiatkowski *et al.*, *Phys. Rev.* **C89**, 045502 (2014).
- [16] J. McCarthy, *Phys. Rev.* **97**, 1234 (1955).
- [17] E. der Mateosian and M. Goldhaber, *Phys. Rev.* **146**, 810 (1966).
- [18] R. Bardin *et al.*, *Nucl. Phys. A* **158**, 337 (1970).
- [19] K. You *et al.*, *Phys. Lett.* **B265**, 53 (1991).
- [20] V. B. Brudanin *et al.*, *Phys. Lett.* **B495**, 63 (2000).
- [21] I. Ogawa *et al.*, *Nuclear Physics A* **730**, 215 (2004).
- [22] S. Umehara *et al.*, *Phys. Rev.* **C78**, 058501 (2008).
- [23] R. Arnold *et al.*, *Phys. Rev. D* **93**, 112008 (2016).
- [24] S. S. Nabiev *et al.*, *Phys. Atomic Nuclei* **64**, 1541 (2001).
- [25] K. Matsuoka *et al.*, *J. Phys. Conf. Series* **1468**, 012199 (2020).
- [26] S. Umehara *et al.*, *Prog. Theor. Exp. Phys.* **053C03**, 1 (2015).
- [27] R. Hazama *et al.*, *KURRI Progress Report* **2016**, 17 (2017).
- [28] T. Kishimoto *et al.*, *Prog. Theor. Exp. Phys.* **033D03**, 1 (2015).
- [29] S. Yoshida *et al.*, *Nucl. Instr. and Meth* **A601**, 282 (2009).
- [30] S. Umehara *et al.*, *Phys. Procedia* **61**, 283 (2015).
- [31] K. Nakajima *et al.*, *AIP Conf. Proc.* **1672**, 110004 (2015).
- [32] T. Iida *et al.*, *Nucl. Part. Phys. Proc.* **273-275**, 2633 (2016).
- [33] T. Iida *et al.*, *J. Phys. Conf. Ser.* **718**, 062026 (2016).
- [34] S. Umehara *et al.*, *PoS INPC2016*, 246 (2017).
- [35] K. Nakajima *et al.*, *Astropart. Phys.* **100**, 54 (2018).
- [36] V. Mikhailik *et al.*, *Nucl. Instr. and Meth* **A566**, 522 (2006).
- [37] B. Khai *et al.*, *IEEE Trans. Nucl. Sci.* **66**, 1174 (2019).

- [38] “-SpaceWire- Links, nodes, routers and networks,” <https://ecss.nl/standard/ecss-e-st-50-12c-rev-1-spacewire-links-nodes-routers-and-networks-15-may-2019/> (2019).
- [39] T. Maeda *et al.*, IEEE Trans. Nucl. Sci. **62**, 1128 (2015).
- [40] K. Suzuki *et al.*, IEEE Trans. Nucl. Sci. **62**, 1122 (2015).
- [41] Y. Yasu *et al.*, IEEE Transactions on Nuclear Science **57**, 487 (2010).
- [42] F. A. Danevich *et al.*, Phys. Rev. C **67**, 014310 (2003).
- [43] T. Iida *et al.*, submitted to Nucl. Instr. and Meth. A (2020), arXiv:2003.13404 [physics.ins-det].
- [44] J. Engel and J. Menéndez, Reports on Progress in Physics **80**, 046301 (2017).